J Nanopart Res (2012) 14:831
DOI 10.1007/s11051-012-0831-7

RESEARCH PAPER

Room temperature biogenic synthesis of multiple nanoparticles (Ag, Pd, Fe, Rh, Ni, Ru, Pt, Co, and Li) by *Pseudomonas aeruginosa* SM1

Sarvesh Kumar Srivastava · Magda Constanti

Received: 13 December 2011 / Accepted: 14 March 2012 / Published online: 31 March 2012

Abstract Room temperature biosynthesis of Ag, Pd, Fe, Rh, Ni, Ru, Pt, Co, and Li nanoparticles was achieved using *Pseudomonas aeruginosa* SM1 without the addition of growth media, electron donors, stabilizing agents, preparation of cell/cell-free extract or temperature, and pH adjustments. The resulting nanoparticles were characterized by Transmission electron microscopy and X-ray diffraction. It was observed that *P. aeruginosa* SM1 is capable of producing both intracellular (Co and Li) and extracellular (Ag, Pd, Fe, Rh, Ni, Ru, and Pt) nanoparticles in both crystalline and amorphous state. The FT-IR spectra clearly showed the presence of primary and secondary amines which may be responsible for the reduction and subsequent stabilization of the resulting extracellular nanoparticles which were obtained as a one-step process. This suggests toward an unknown "selection mechanism" that reduces certain metal ions and allows others to enter the cell membrane. Finally, in this first of its kind study, single strain of bacteria was used to produce several different mono-metallic nanoparticles.

Keywords Nanoparticles · Biosynthesis · Nanotechnology · Green chemistry · *Pseudomonas aeruginosa*

S. K. Srivastava · M. Constanti (✉)
Departament d'Enginyeria Química, Universitat Rovira i Virgili, Av. Països Catalans 26, 43007 Tarragona, Spain
e-mail: magdalena.constanti@urv.cat

Introduction

In recent years, the use of biological systems has emerged as a radical technology for synthesizing nanoparticles with an aim to control nanoparticle morphology and monodispersity. Bacteria are an exciting category of microorganisms which have an innate ability to reduce metallic ions to their respective metallic nanoparticles and function as cost-effective "green" nanofactories. This reduction mechanism in bacteria is due to their chemical detoxification acting as a defence (Hallmann et al. 1997) mechanism as well as due to energy-dependent ion efflux from the cell by membrane proteins that function either as ATPase or ion-transporters (Bruins et al. 2000). In fact, interactions between metals and microbes have been used for such biological applications (Klaus-Joerger et al. 2001) as biomineralization, bioremediation, bioleaching, and biocorrosion. The microbial synthesis of nanoparticles has emerged as a promising field of research that bridges applied microbiology and nanotechnology.

It should be noted that there are various physical and chemical methods which are used to produce monodisperse metallic nanoparticles by including surfactants (for stability) and use of toxic chemicals (reductants, solvents, etc.). Therefore, there is an immediate need for an effective alternative. The use of toxic chemicals on the surface of nanoparticles and non-polar solvents in their synthesis limits application in the clinical field. Therefore, the development of

non-toxic, clean, and bio-compatible nanoparticles is a welcome sign. Bacteria can produce nanoparticles both intracellularly and extracellularly as shown in Table 1.

It is interesting that nanoparticles are increasingly being synthesized by bacteria even though the exact mechanism is still unclear (Zhang et al. 2011). Some of the studies mentioned above (Table 1) suggested that bacterial nanoparticle synthesis depends on factors such as strain type, physical conditions like pH, time and temperature, and the type and concentration of the metallic salt. The growing demand for nanoparticles can indeed be supplied by a cost-effective green synthesis from biological systems. Thus, extracellular production of metal nanoparticles has greater commercial application than intracellular nanoparticles as they are easier to extract and process.

Silver nanoparticles have found tremendous usage as antimicrobial agents and are extensively used in surgical utilities, paints, water filters, clothing, etc. (Rai et al. 2009; Son et al. 2004). Palladium nanoparticles are widely used in various catalytic reactions along with the fabrication of hydrogen sensing equipment (Gopidas et al. 2003). Various studies have conclusively supported the use of iron nanoparticles in the cleaning of contaminated land and waters (Huber 2005), and iron oxide probes are also being used in molecular imaging processes (Artemov et al. 2003). Rhodium, platinum, and ruthenium nanoparticles are widely used in various catalytic processes and have provided break-through technology in energy production from fuel cells (Mu et al. 2005; Liu et al. 2004; Zhang and Chan 2003). While nickel and lithium nanoparticles are widely used in the fabrication of alloys and catalysis (Molenbroek and Nørskov 2001; Kima et al. 2007), cobalt nanoparticles have been used in such important surface chemistry modifications as the formation of polymer microspheres (Cui et al. 2005).

We describe here the first demonstration of extracellular synthesis of silver (Ag), palladium (Pd), platinum (Pt), iron (Fe), rhodium (Rh), nickel (Ni), and ruthenium (Ru) as a one-step process from a single strain of bacteria *Pseudomonas aeruginosa* SM1. The same strain was used to produce intracellular nanoparticles of cobalt (Co) and lithium (Li). The resulting nanoparticles were obtained in high yield with a well-defined size, shape, and dispersity with no addition of such stabilizing agents as surfactants or any kind of pH/temperature adjustment throughout the process. This study discusses the particle characterization of various metallic nanoparticles and some interesting details about the synthesis of bacterial nanoparticle.

Materials and methods

Bacterial strain and growth conditions

P. aeruginosa SM1 cells were procured from our existing strain collection. The strain was originally isolated from a natural aqueous environment and then subjected to 16S rDNA gene sequencing. The *P. aeruginosa* SM1 strain was cultured in 50-mL nutrient broth (10 g/L peptone, 10 g/L meat extract, and 0.5 g/L NaCl) at 27 °C and 120 rpm overnight in screw-cap flasks. After a day of incubation, the culture was centrifuged at 10,000 rpm for 10 min, and the resulting bacterial pellet was separated and retained. The bacterial pellet was thoroughly washed three times in sodium saline solution and then three times in MilliQ water to remove any unwanted material sticking to the

Table 1 List of bacteria that synthesize metal nanoparticles

Microorganism	Nanoparticle	Localization	Reference
Bacillus subtilis 168	Au	Inside the cell wall	Lengke and Southam (2006)
Shewanella algae	Au	Periplasmic space	Konishi et al. (2007)
Pseudomonas stutzeri AG259	Ag	Periplasmic space	Joerger et al. 2000
Bacillus sp.	Ag	Periplasmic space	Pugazhenthiran et al. (2009)
Corynebacterium sp. SH09	Ag	Cell wall	Zhang et al. (2005)
Shewanella oneidensis MR-1	Pd	Periplasmic space	De Windt et al. (2005)
Desulfovibrio desulfuricans	Pd	Cell surface	Yong et al. (2002)
Aquaspirillum magnetotacticum	Fe	Inside the cell wall	Mann et al. (1984)

cells. These washed cells were then weighed and 0.2 g wet weight pellets were prepared for every 50 mL of salt solution. The washed cells suspended in 10 mL distilled water gave a solution with cell concentration of about 3.2×10^{11} cells/mL. Similar technique was employed by Husseiny et al. (2007).

Synthesis of biogenic nanoparticles

Uniform solutions of 0.001 M were prepared from silver nitrate ($AgNO_3$), disodium tetrachloropalladate (Na_2PdCl_4), iron(III) nitrate ($Fe(NO_3)_3$), sodium hexachloro rhodate(III) dihydrate ($Na_3RhCl_6{\cdot}2H_20$), nickel(II) chloride ($NiCl_2{\cdot}6H_2O$), ammonium hexachlororuthenate(IV) ($(NH_4)_2RuCl_6$), ammonium hexachloroplatinate(IV) ($(NH_4)_2PtCl_6$), cobalt(II) chloride hexahydrate ($CoCl_2{\cdot}6H_2O$), and lithium chloride (LiCl). It should be noted that the pH was not subsequently adjusted. There were two control solutions for each salt: a salt solution with no inoculum and a salt solution with heat-killed cells as inoculum. Finally, the 0.2 g cell pellet was introduced separately into each of the 50 mL of 0.001 M salt. Each of these reaction mixtures and the respective controls were kept under static conditions at the typical room temperature of 25 °C. At the end of the reaction time (24 h, previously measured by synthesis of gold nanoparticle experiments (data not shown)), the cells were removed by centrifugation at 4,000 rpm for 10 min and the resulting supernatant was used for further analytical studies. We observed that at lower salt concentration and lower cell concentration, relative homogeneity of the nanoparticle solution was found to be maintained.

For intracellular nanoparticles, including lithium and cobalt, an additional extraction step was performed after 24 h for the TEM imaging of nanoparticles. A total of 10 mL from each reaction mixture was separately mixed with ethanol in 1:1 ratio followed by vortexing for 2 min. This caused the bacterial cell wall to lyze and the intracellular metal nanoparticle came out in the reaction mixture. This step was followed by adding 10 mL of hexane and vortexing for 2 min. The top layer, comprising of hexane and liberated metal particle, was pipetted out and stored.

Characterization of biogenic nanoparticles

The morphology and grain size of the resulting nanoparticles were analyzed using a Jeol JEM 1011 electron microscope (TEM) connected to a high resolution imaging system. A total of 2 μL was taken from the two reaction mixtures, placed on carbon-coated copper grids, and dried at room temperature. The images were obtained by Olympus iTEM Imaging Software and were further analyzed using ImageJ 1.43 M software.

A Fourier transformation–infrared spectroscopy (FT-IR) analysis was done using a Jasco FT/IR-680 plus coupled to a high performance computer. The samples (100 μL) were placed in the ATR analyzer, and the resulting spectra were analyzed using Spectra Manager ver. 1.06.02. The FT-IR spectrum of each reaction mixture was interpreted as per Silverstein et al. (2005).

X-ray diffraction (XRD) measurements were made using a Siemens D5000 diffractometer (Bragg–Brentano parafocusing geometry and vertical θ–θ goniometer) fitted with a curved graphite diffracted-beam monochromator and diffracted-beam Soller slits, a 0.06° receiving slit and scintillation counter as a detector. The angular 2θ diffraction range was between 25 and 100°. A drop of the sample (100 μL) was deposited on to a low background Si (510) sample holder. The data were collected with an angular step of 0.05° at 12 s per step and sample rotation. Cukα radiation was obtained from a copper X-ray tube operated at 40 kV and 30 mA. The chemical nature of metallic nanoparticles was analyzed by Diffracplus Evaluation software (Bruker 2007), which compared the XRD diffractograms with the ICDD data base.

Results and discussion

This study explores the synthesis of numerous metallic nanoparticles by *P. aeruginosa* SM1. The reaction mixture of ionic solutions (metal salts) along with their respective controls were analyzed primarily by TEM. As expected, none of the control solutions (heat-killed cells and without inoculum) gave a positive result and were excluded from further analysis by FT-IR and XRD.

Figure 1(a–i) presents the TEM images of the nanoparticles produced from silver, palladium, iron, rhodium, nickel, ruthenium, platinum, cobalt, and lithium, respectively. It is interesting to note that silver nanoparticles (Fig. 1a) are considered to be a potent antibacterial agent. However, some reports have

described the production of silver nanoparticles using bacteria (see above) with their particle characterization. The silver nanoparticles obtained were fairly dispersed and of size 6.3 ± 4.9 nm. The TEM images show smaller particles in form of spheres, while the larger particles tend to form disks. The palladium nanoparticles (Fig. 1b) were considerably larger (around 22.1 ± 6.2 nm) and were dense polygons in shape. The presence of iron nanoparticles (Fig. 1c) was revealed by the fact that the color of the reaction mixture changed from colorless to slightly orange, which indicated presence of iron oxide. These highly dispersed flake-like particles were of 20.5 ± 5.3 nm in size. As far as we know, this is the first reporting for the synthesis of rhodium nanoparticles by any living system. Fig 1d shows the extracellular rhodium nanoparticles as small dense particles of size 2.1 ± 0.9 nm. It is interesting to note that the resulting particles were very small which might be the reason of particle aggregation observed by TEM. Biogenic synthesis of Ni nanoparticle was achieved for the first time by a bacterial system. The observed nickel nanoparticles (Fig. 1 e) were of discrete form and measured 2.9 ± 1.2 nm. However, unlike rhodium nanoparticles, they were better dispersed and maintained their shape in the reaction mixture. Just like rhodium and nickel nanoparticles, ruthenium nanoparticles (Fig. 1f) were also produced for the first time by a living system. It was observed that the resulting nanospheres (and occasional disks) of size 8.3 ± 5.4 nm were well dispersed with perfect circularity (spheres) for all particle size. The lack of particle aggregation also suggested that they are inherently stable in the reaction mixture. Platinum nanoparticles (Fig. 1g) were produced measuring about 450 nm in the form of unit circular disks. Another study conducted by Riddina et al. (2010) showed similar results (large particle size) with cell-free extract of

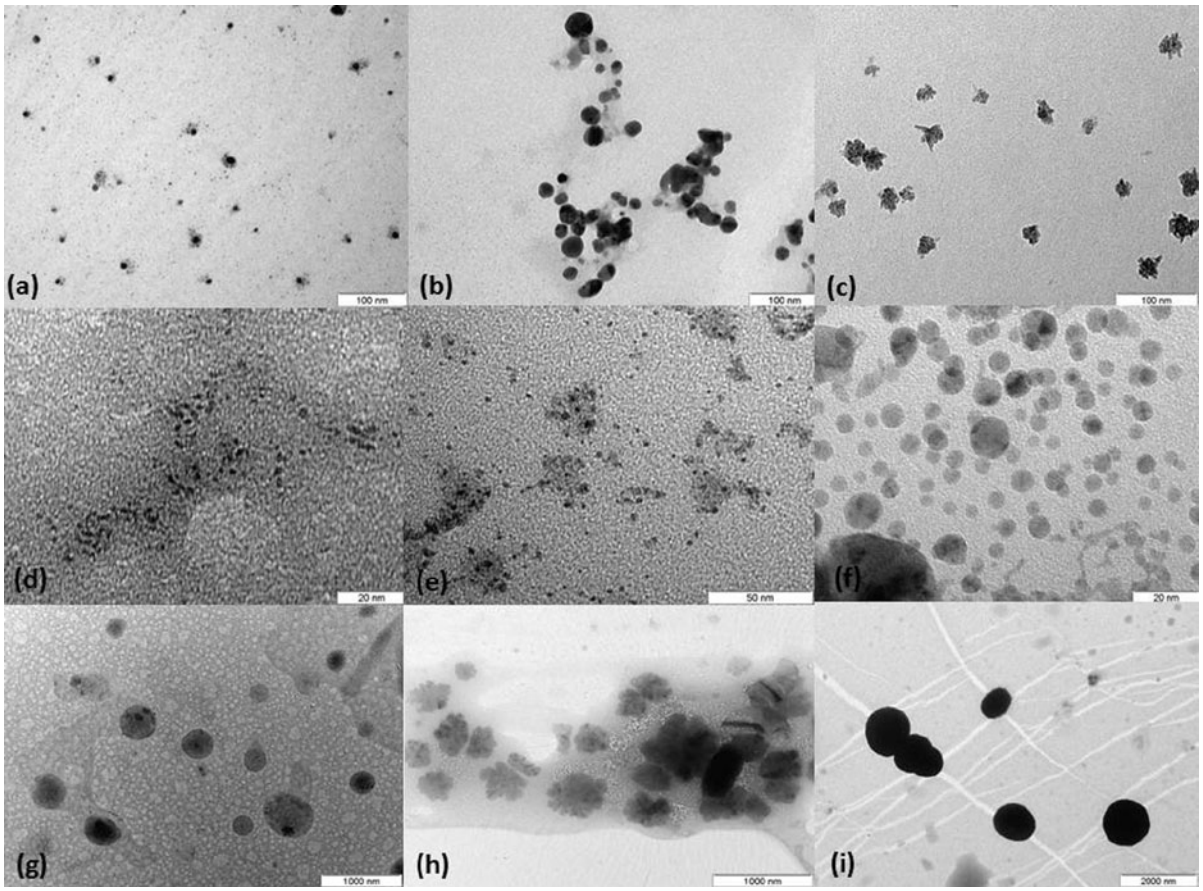

Fig. 1 TEM analysis of biogenic nanoparticles after 24 h: **a** Ag, **b** Pd, **c** Fe, **d** Rh, **e** Ni, **f** Ru, **g** Pt, **h** Co, **i** Li

sulfate reducing bacteria (SRB) to produce cuboid platinum nanoparticles of size 200–1,000 nm. The large particle size can be attributed to the fact that platinum salts are generally sparingly soluble/insoluble in water. Thus, they have a strong tendency to accumulate/cluster together in the course of reaction resulting in larger particle size.

Finally, the two intracellular nanoparticles produced in this study were cobalt (Fig. 1h) and lithium (Fig. 1i). Figure 2 clearly shows cobalt and lithium nanoparticles inside the bacterial cell as observed by TEM. After the ethanol–hexane-mediated extraction of these intracellular nanoparticles, it was observed that the resulting nanoparticles differ considerably in terms of shape and size.

Cobalt nanoflakes were 550 nm in size (approx.), while lithium nanoparticles were highly dense and circular with 750 nm in size (approx.). These intracellular nanoparticles were well-packed inside the bacterial cell. Therefore, when the cell lysed, the true shape of the nanoparticle was observed to be different than when packed inside the cell. In Fig. 2 (a) the encircled region shows the intracellular deposition of cobalt which showed flake-like form (Fig. 2b) after cell lysis. Similarly, the resulting dense spherical type lithium nanoparticles (Fig. 2d) appeared oval inside the cell (see the highlighted region of Fig. 2c). It is interesting to note that vitamin B12 (cobalamin) is synthesized by *Pseudomonas* sp. (Kuroda et al. 2004). This suggests that either an underlying defence/transport mechanism allows cobalt ions to enter the cell or the lipopolysaccharide (LPS)/cell wall facilitates specific ion uptake. Other studies also suggest that there is a unique lithium mediated ion transport system present in *P. aeruginosa* in the high-salt region (Blanche et al. 1991). Therefore, the two intracellular nanoparticles (Li and Co) suggests that there may be a unique "selection mechanism" present in this bacterium allowing certain ions to pass, while "reducing" others in its vicinity. This was further supported by FT-IR spectra which suggested that certain primary and secondary amines are responsible for the extracellular synthesis of metallic nanoparticles although the same was not observed for intracellular nanoparticles. Table 2 shows all the nanoparticles analyzed by TEM with data about the number of particles observed, shape and size.

The FT-IR spectra of all the extracellularly produced nanoparticle (Ag, Pd, Fe, Rh, Ni, Ru, and Pt) solutions showed a remarkable resemblance with each

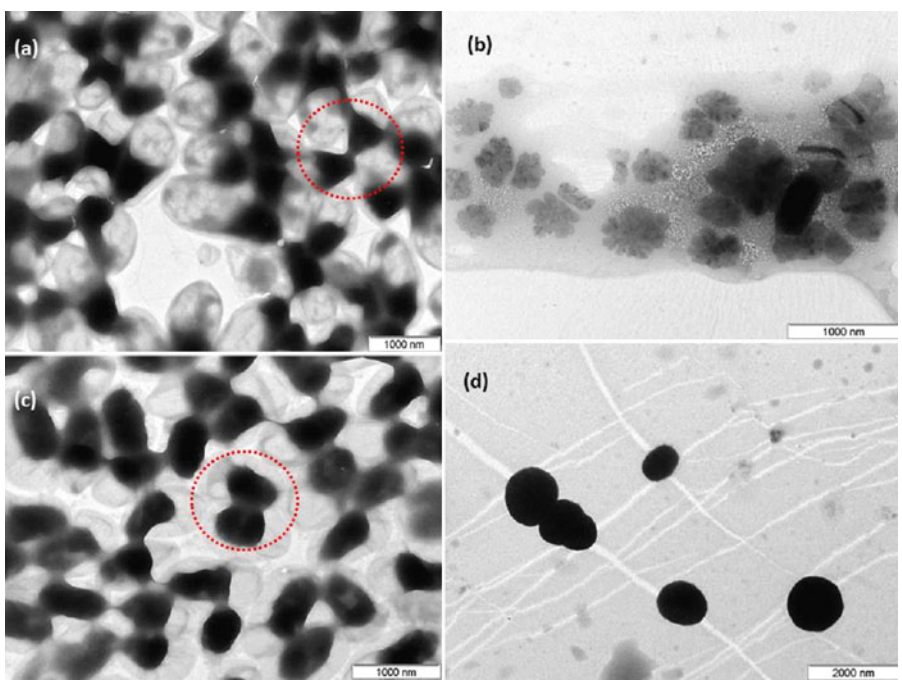

Fig. 2 TEM images of Co nanoparticles: **a** trapped inside the cell **b** extracellularly; TEM images of Li nanoparticles **c** trapped inside the cell **d** extracellularly

other. Three major bond stretchings were clearly observed (Fig. 3) in all the seven extracellularly produced nanoparticles which were in the range 3,600–3,400 cm^{-1}(1), 2,800–3,000 cm^{-1}(2), and 1,000–1,400 cm^{-1}(3). The peak stretchings in the region 3,400–3,100 cm^{-1} were primarily of OH groups which were present because of the water and were more prominently observed in the silver,

Table 2 Biogenic nanoparticles synthesized by *P. aeruginosa* SM1

Serial no.	NP type	Particle size (nm)	No. of particles observed	Shape	Other info
1	Ag	6.3 ± 4.9	150	Spheres and disks	Extracellular
2	Pd	22.1 ± 6.2 nm	16	Polygons and disks	Extracellular
3	Fe	20.5 ± 5.3	77	Largely flakes	Extracellular
4	Rh	2.1 ± 0.9	22	Dense polygons	Extracellular
5	Ni	2.9 ± 1.2	75	Dense polygons	Extracellular
6	Ru	8.3 ± 5.4	251	Spheres and some disks	Extracellular
7	Pt	450 (approx)	15	Spheres with a few disks	Extracellular
8	Co	550 ± 100	20	Flakes	Intracellular
9	Li	950 ± 150	6	Polygons and disks	Intracellular

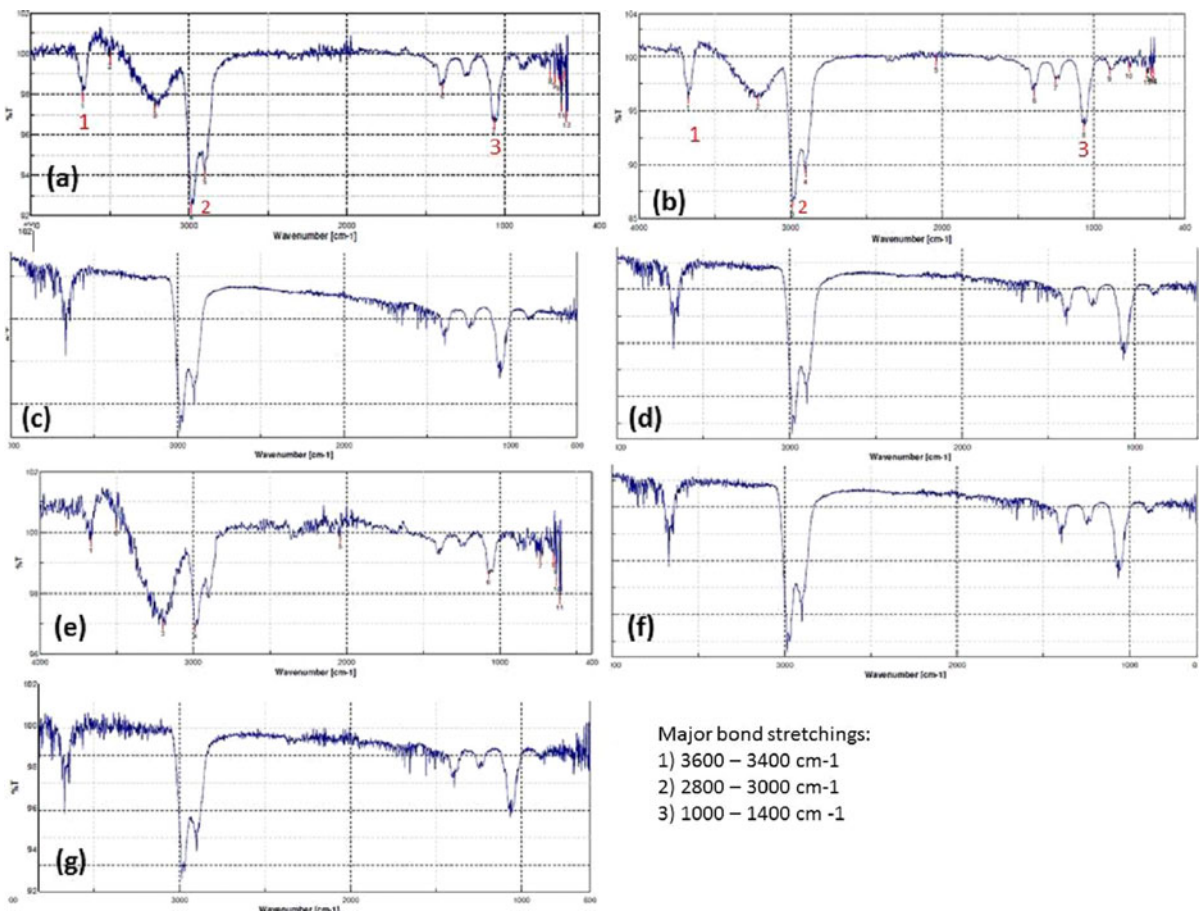

Fig. 3 FT-IR spectra of extracellular nanoparticle solutions: **a** silver, **b** palladium, **c** iron, **d** rhodium, **e** nickel, **f** ruthenium, **g** platinum

palladium, and nickel nanoparticle solution (suggesting the presence of intermolecular H-bonds). Although the actual peak values differed slightly in all the reaction mixtures, they all followed the same range (see above) and gave meaningful insights into the probable mechanism of extracellular nanoparticle synthesis and its subsequent stabilization. It is interesting to note that the peak values in the region 3600–3400 cm^{-1} also strongly correspond to the presence of primary amines in solution. Further, the band in this region tends to shift to longer wavelengths by hydrogen bonding, which can be observed in all the spectral data. The aliphatic C-chain stretch is very sharp and distinct between 3,000 and 2,800 cm^{-1} suggesting the presence of CH and CH_2 groups along with the probable C–N stretch around the 1,070 cm^{-1} region. The fact that medium-to-weak absorption bands for the unconjugated C–N linkage in primary, secondary, and tertiary amines appear in the region of 1,250–1,020 cm^{-1} reinforces this suggestion. Further, the weak broken band around 1,400 cm^{-1} may be the result of a C–N stretching band of primary amides formed during the course of the reaction. The FT-IR spectra clearly suggests that certain organic compounds consisting of amino acids are involved in the reaction and may also be responsible for subsequent stabilization of the resulting extracellular nanoparticles. Also, the absence of active groups (carbon chains or amines) in the FT-IR spectra (Fig. 4) of two intracellular reaction mixtures (Co and Li) suggests that the reduction mechanism observed for extracellular nanoparticles synthesis may not be just some random extracellular synthesis of certain proteins, but a coordinated response from the cell depending upon the type of metal ion present in the solution.

The absence of any organic band in the FT-IR spectra of intracellular nanoparticles also suggests that these ions (cobalt and lithium) were "allowed" to enter the cell unlike the extracellular nanoparticles, in which the ions were reduced by some unknown mechanism present in *P. aeruginosa* SM1. Further research is required to corroborate this hypothesis and provide more information about the molecular basis of this reduction mechanism.

Finally, the chemical composition of the resulting nanoparticles was analyzed by SAED (Selected area

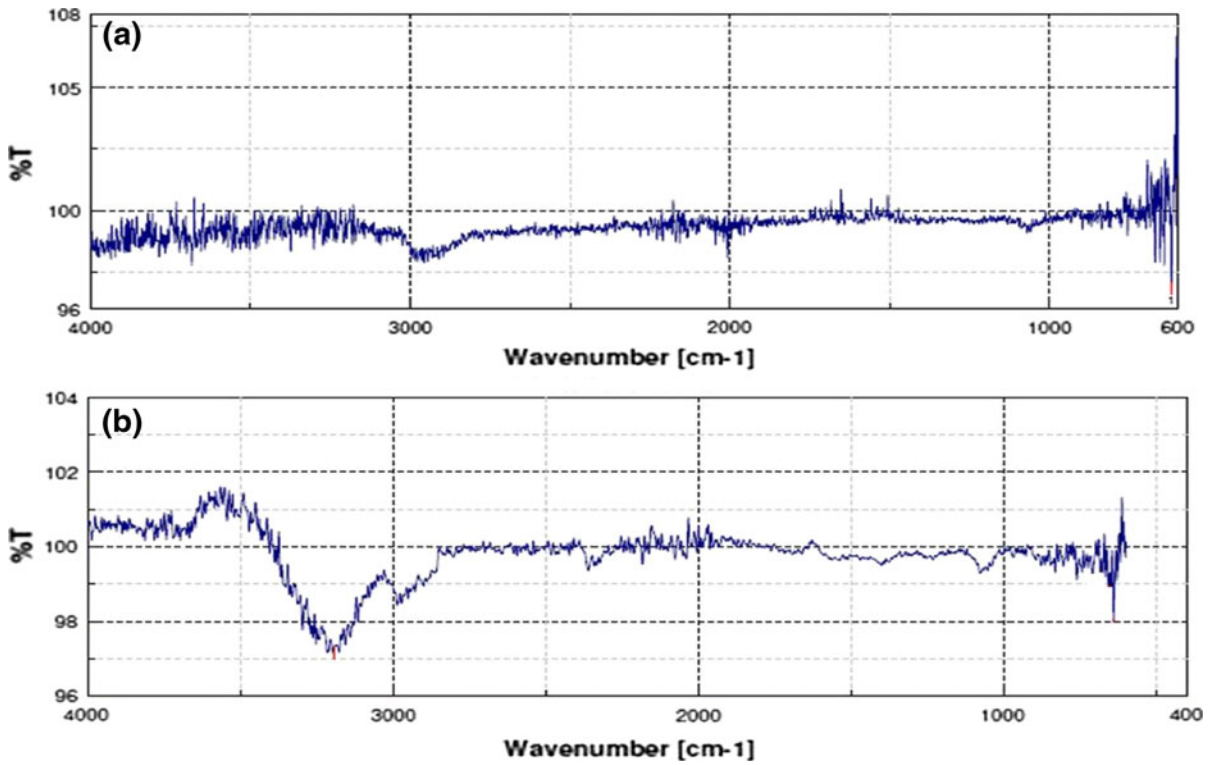

Fig. 4 FT-IR spectra of intracellular nanoparticle solutions **a** Li and **b** Co

electron diffraction) and XRD. It was interesting to note that the ruthenium, rhodium, cobalt, nickel, and lithium nanoparticles in the solution synthesized by *P. aeruginosa* SM1 were found to be amorphous by SAED (data not shown). As XRD can provide diffractograms only for crystalline materials, the diffractogram of amorphous nanoparticle solution (Ru, Rh, Co, Ni, and Li) were only noise and are not presented in this study. All the other crystalline nanoparticles (Ag, Fe, Pd, and Pt) were observed by XRD and their chemical composition was determined accordingly. The XRD spectra of silver nanoparticle solution showed distinct presence of silver oxide (AgO) as the reduced metallic form of silver (see Fig. 5a). Thus, the silver ions were reduced to their oxide state in the presence of *P. aeruginosa* SM1. The diffractogram of the iron nanoparticle solution (Fig. 5b) confirmed the presence of hydrohematite (i.e., FeO(OH)). It should be pointed out that this distinct brown-orange tint of the reduced solution suggests the state of iron which is also formed when iron-containing substances rust under water. In the absence of any antioxidant to prevent the rusting of iron nanoparticles, the presence of hydrohematite (i.e., FeO(OH)) was confirmed by its XRD spectra.

The XRD pattern of palladium nanoparticle solution marked the peaks for synthesized metal palladium (Fig. 5c) in the reaction solution. It should be noted that palladium metal does not react with oxygen at normal temperatures (only at 800 °C or above) (Craig and Anderson 1995), which explains why only synthesized palladium was detected in the diffractogram and not its oxide/hydroxide. For the platinum nanoparticle solution, XRD identified three distinct compounds as synthesized platinum, platinum chloride, and methylamine chloroplatinate. Also, platinum is generally insoluble in water, hydrochloric acid, and nitric acid, and tends to form halogenated compounds with chlorine (Lide and David 2007). This presence of chloride and chloroplatinate is explained by the fact that the starting ionic solution was also a halogenated compound (ammonium chloroplatinate) before reduction.

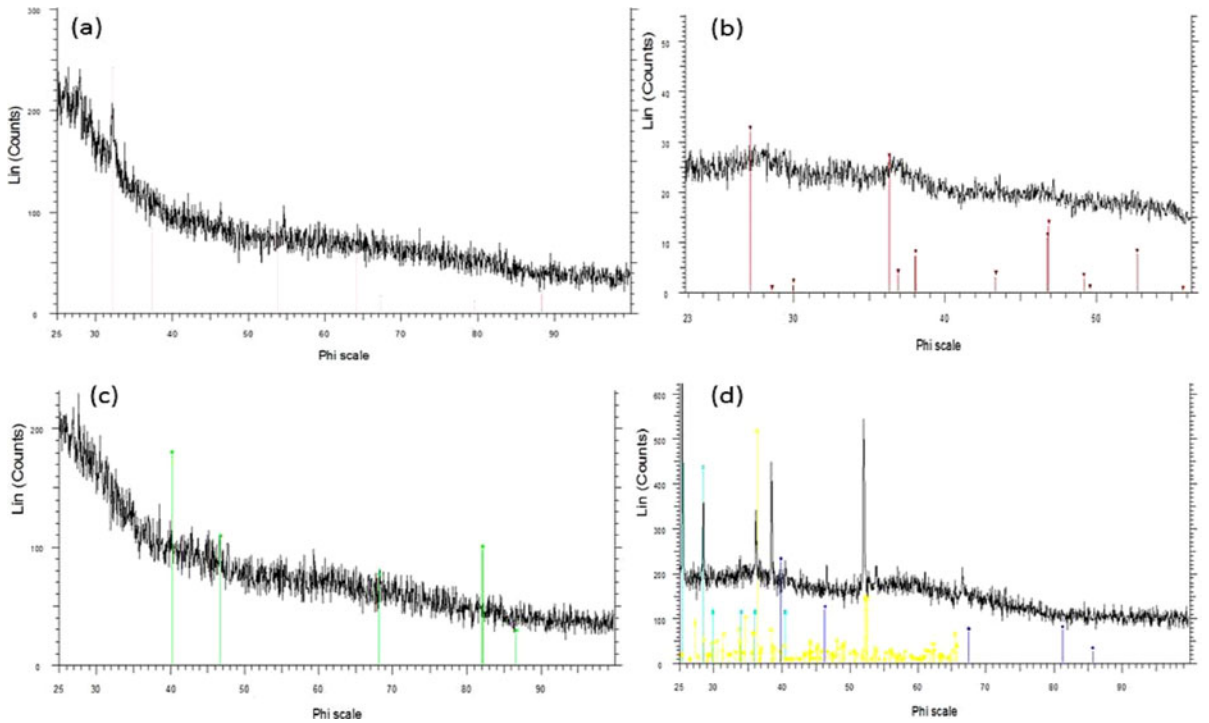

Fig. 5 Diffractograms obtained from nanoparticle solutions: **a** silver, *highlighted region* corresponds to the presence of AgO; **b** Iron, *highlighted region* corresponds to the presence of FeO(OH); **c** palladium, *highlighted region* corresponds to the presence of synthesized palladium metal; **d** platinum (the *blue*, *yellow* and *green highlighted regions* correspond to methylamine chloroplatinate, $PtCl_3$ and synthesized platinum, respectively. (Color figure online)

The resulting nanoparticles were observed to be well dispersed and of discrete shape and size. It is important to note that the exact mechanism and the site/mode of synthesis for biogenic nanoparticles is currently being investigated, and this study explores a new perspective. Interestingly, many biogenic nanoparticle studies deal with the synthesis of gold nanoparticles (Ogi et al. 2010; Bhambure et al. 2009; Husseiny et al. 2007). This may be because gold is a noble metal and is quickly reduced even under mild reducing conditions as is the case of biological systems. Also, reduced elemental gold can be easily detected by XRD because it tends to form a crystalline structure.

Finally, with the help of FT-IR data we successfully highlighted the presence of certain functional groups which may be responsible for reducing metal ions into their respective nanoparticles. We also used XRD to demonstrate that the nanoparticle being synthesized can be amorphous or crystalline. It was interesting to note that both the intracellular nanoparticles (cobalt and lithium) were amorphous suggesting that they had been formed and deposited intracellularly. With eight d-block elements (Ru, Rh, Ni, Co, Pd, Pt, Fe, and Ag) and one s-block element (Li) we were able to synthesize and characterize various biogenic nanoparticles from a single strain of bacteria.

Conclusions

With increasing demand for engineered nanomaterials, it becomes important to develop eco-friendly strategies for their fabrication with an aim to develop economically viable synthesis routes. This study shows extracellular nanoparticle synthesis of Ag, Pd, Fe, Rh, Ni, Ru, and Pt as a one-step process by *P. aeruginosa* SM1. The two intracellular nanoparticles (Co and Li) were also produced which required an additional extraction procedure. The "cost-effective and simple" objective which is generally required for commercialization is highlighted by the fact that this study was carried out without the addition of nanoparticle stabilizing surfactants or control of pH or temperature at any point throughout the investigation. TEM images confirm the presence of biogenic nanoparticles with fixed shape, size, and dispersity. Spherical/disk type conformations were obtained for Ag (6.3 ± 4.9 nm), Ru (8.3 ± 5.4 nm), and Pt (450 nm), while Pd (22.1 ± 6.2 nm) and Li (950 nm; intracellular) showed polygons and disks, respectively. Also, small and dense polygons were observed in case of Rh (2.1 ± 0.9 nm) and Ni (2.9 ± 1.2 nm) nanoparticles. Flake type conformation was observed in the case of Fe (20.5 ± 5.3 nm) and Co (550 nm; intracellular) nanoparticles. Further, it was concluded that the resulting biogenic nanoparticles were amorphous (Ru, Rh, Co, Ni, and Li) and crystalline (Ag, Fe, Pd, and Pt). XRD gave important information about the structural composition of crystalline nanoparticles. FT-IR spectra detected no chemical groups in the intracellular nanoparticles, but did in the extracellular nanoparticles. Finally, this "single strain-multiple particles" synthesis has the potential to revolutionize the production of nanoparticles and requires interdisciplinary research. The usefulness of these different metallic nanoparticles generated through one-step biological synthesis is tremendous and will find numerous applications in the field of catalysis, electrochemistry, chemical synthesis, and biomedicine.

Acknowledgments We would like to thank the Spanish Ministry of Science and Innovation for its financial support through the Grant BIO2008-02841.Our gratitude also goes to Dr. Francesc Gispert Guirado of the Scientific and Technical Resources Service of the URV (Tarragona) for his help with the X-ray diffraction analyses.

References

Artemov D, Mori N, Okollie B, Bhujwalla ZM (2003) MR molecular imaging of the Her-2/neu receptor in breast cancer cells using targeted iron oxide nanoparticles. Magn Reson Med 49:403–408

Bhambure R, Bule M, Shaligram N, Kamat M, Singhal R (2009) Extracellular biosynthesis of gold nanoparticles using *Aspergillus niger*—its characterization and stability. Chem Eng Technol 32:1036–1041

Blanche F, Couder M, Debussche L, Thibaut D, Cameron B, Crouzet J (1991) Biosynthesis of vitamin B12: stepwise amidation of carboxyl groups b, d, e, and g of cobyrinic acid a,c-diamide is catalyzed by one enzyme in *Pseudomonas denitrificans*. J Bacteriol 173:6046–6051

Bruins RM, Kapil S, Oehme SW (2000) Microbial resistance to metals in the environment. Ecotoxicol Environ Saf 45:198–207

Craig BD, Anderson DS (1995) Atmospheric environment: handbook of corrosion data. ASM International p 126

Cui H, Zayat M, Levy D (2005) Nanoparticle synthesis of willemite doped with cobalt ions (Co0.05Zn1.95SiO4) by an epoxide-assisted sol–gel method. Chem Mater 17:5562–5566

De Windt D, Aelterman P, Verstraete W (2005) Bioreductive deposition of palladium (0) nanoparticles on *Shewanella oneidensis* with catalytic activity towards reductive

dechlorination of polychlorinated biphenyls. Environ Microbiol 7:314–325

Gopidas KR, Whitesell JK, Fox MA (2003) Synthesis, characterization, and catalytic applications of a palladium-nanoparticle-cored dendrimer. Nano Lett 3:1757–1760

Hallmann J, Hallmann AQ, Mahaffee WF, Kloepper JW (1997) Bacterial endophytes in agricultural crops. Can J Microbiol 43:895–914

Huber DL (2005) Synthesis, properties, and applications of iron nanoparticles. Small 1:482–501

Husseiny MI, Abd El-Aziz M, Badr Y, Mahmoud MA (2007) Biosynthesis of gold nanoparticles using *Pseudomonas aeruginosa*. Spectrochim Acta A 67:1003–1006

Joerger R, Klaus T, Granqvist CG (2000) Biologically produced silver-carbon composite materials for optically functional thin-film coatings. Adv Mater 12:407–409

Kima TR, Kima DH, Ryua HW, Moona JH, Leeb JH, Boob S, Kim J (2007) Synthesis of lithium manganese phosphate nanoparticle and its properties. J Phys Chem Solids 68:1203–1206

Klaus-Joerger T, Joerger R, Olsson E, Granqvist CG (2001) Bacteria as workers in the living factory: metal-accumulating bacteria and their potential for materials science. Trends Biotechnol 19:15–20

Konishi Y, Tsukiyama T, Tachimi T, Saitoh N, Nomura T, Nagamine S (2007) Microbial deposition of gold nanoparticles by the metal-reducing bacterium *Shewanella algae*. Electrochim Acta 53:186–192

Kuroda T, Fujita N, Utsugi J, Kuroda M, Mizushima T, Tsuchiya T (2004) A major Li(+) extrusion system NhaB of *Pseudomonas aeruginosa*: comparison with the major Na(+) extrusion system NhaP. Microbiol Immunol 48: 243–250

Lengke M, Southam G (2006) Bioaccumulation of gold by sulfate-reducing bacteria cultured in the presence of gold(I)-thiosulfate complex. Geochim Cosmochim Acta 70:3646–3661

Lide I, David R (2007) Platinum. CRC handbook of chemistry and physics, 4th edn. CRC Press, New York

Liu Z, Ling XY, Su X, Lee JY (2004) Carbon-supported Pt and PtRu nanoparticles as catalysts for a direct methanol fuel cell. J Phys Chem B 108:8234–8240

Mann S, Frankel RB, Blakemore RP (1984) Structure, morphology, and crystal growth of bacterial magnetite. Nature 310:405–407

Molenbroek AM, Nørskov JK (2001) Structure and reactivity of Ni–Au nanoparticle catalysts. J Phys Chem B 105: 5450–5458

Mu XD, Meng JQ, Li ZC, Kou Y (2005) Rhodium nanoparticles stabilized by ionic copolymers in ionic liquids: long lifetime nanocluster catalysts for benzene hydrogenation. J Am Chem Soc 127:9694–9695

Ogi T, Saitoh N, Nomura T, Konishi Y (2010) Room-temperature synthesis of gold nanoparticles and nanoplates using *Shewanella algae* cell extract. J Nanopart Res 12:2531–2539

Pugazhenthiran N, Anandan S, Kathiravan G, Prakash NKU, Crawford S, Ashokkumar MJ (2009) Microbial synthesis of silver nanoparticles by *Bacillus* sp. J Nanopart Res 11:1811–1815

Rai M, Yadava A, Gadea A (2009) Silver nanoparticles as a new generation of antimicrobials. Biotechnol Adv 27:76–83

Riddina T, Gerickeb M, Whiteleya CG (2010) Biological synthesis of platinum nanoparticles: effect of initial metal concentration. Enzyme Microbiol Technol 46:501–505

Silverstein RM, Webster FX, Kiemle D (2005) Spectrometric identification of organic compounds, 7th edn. Wiley, New York, pp 101–108

Son WK, Youk JH, Lee TS, Park WH (2004) Preparation of antimicrobial ultrafine cellulose acetate fibers with silver nanoparticles. Macromol Rapid Commun 25:1632–1637

Yong P, Rowsen NA, Farr JPG, Harris IR, Macaskie LE (2002) Bioreduction and biocrystallization of palladium by *Desulfovibrio desulfuricans*. Biotechnol Bioeng 80:369–379

Zhang X, Chan KY (2003) Water-in-oil microemulsion synthesis of platinum–ruthenium nanoparticles, their characterization and electrocatalytic properties. Chem Mater 15:451–459

Zhang H, Li Q, Lu Y, Sun D, Lin X, Deng X et al (2005) Biosorption and bioreduction of diamine silver complex by *Corynebacterium*. J Chem Technol Biotechnol 80:285–290

Zhang X, Yan S, Tyagi RD, Surampalli RY (2011) Synthesis of nanoparticles by microorganisms and their application in enhancing microbiological reaction rates. Chemosphere 82:489–494